The Stark effect in Rydberg states of a highly polar diatomic molecule: CaF

Citation: Petrovic#, Vladimir S. et al. "The Stark Effect in Rydberg States of a Highly Polar Diatomic Molecule: CaF." The Journal of Chemical Physics 131.6 (2009) : 064301. © 2009 American Institute of Physics

As Published: http://dx.doi.org/10.1063/1.3179942

Publisher: American Institute of Physics

Persistent URL: http://hdl.handle.net/1721.1/65894

Version: Final published version: final published article, as it appeared in a journal, conference proceedings, or other formally published context

The Stark effect in Rydberg states of a highly polar diatomic molecule: CaF

Vladimir S. Petrović, Jeffrey J. Kay, Stephen L. Coy, and Robert W. Field[a)]
Department of Chemistry, Massachusetts Institute of Technology, Cambridge, Massachusetts 02139, USA

(Received 10 October 2008; accepted 25 June 2009; published online 10 August 2009)

The Stark effect in molecular Rydberg states is qualitatively different from the Stark effect in atomic Rydberg states because of the anisotropy of the ion core and the existence of rotational and vibrational degrees of freedom. These uniquely molecular features cause the electric-field-induced decoupling of the Rydberg electron from the body frame to proceed in several stages in a molecule. Because the transition dipole moment among the same-n^* Rydberg states is much larger than the permanent dipole moment of the ion core, the decoupling of the Rydberg electron from the ion core proceeds gradually. In the first stage, analyzed in detail in this paper, ℓ and N are mixed by the external electric field, while N^+ is conserved. In the further stages, as the external electric field increases, N^+, n^*, and v^+ are expected to undergo mixing. We have characterized these stages in $n^*=13$, $v^+=1$ states of CaF. The large permanent dipole moment of CaF^+ makes CaF qualitatively different from the other molecules in which the Stark effect in Rydberg states has been described (H_2, Na_2, Li_2, NO, and H_3) and makes it an ideal testbed for documenting the competition between the external and CaF^+ dipole electric fields. We use the weak-field Stark effect to gain access to the lowest-N rotational levels of f, g, and h states and to assign their actual or nominal N^+ quantum number. Lowest-N rotational levels provide information needed to disentangle the short-range and long-range interactions between the Rydberg electron and the ion core. We diagonalize an effective Hamiltonian matrix to determine the ℓ-characters of the $3 \leqslant \ell \leqslant 5$ core-nonpenetrating $^2\Sigma^+$ states and to characterize their mixing with the core-penetrating states. We conclude that the mixing of the $\ell=4$, $N-N^+=-4(g(-4))$ state with lower-ℓ $^2\Sigma^+$ states is stronger than documented in our previous multichannel quantum defect theory and long-range fits to zero-field spectra. © *2009 American Institute of Physics*. [DOI: 10.1063/1.3179942]

I. INTRODUCTION

Since its discovery in 1913, the Stark effect has been widely used to probe and exert control over atoms and molecules. The Stark effect in Rydberg states has received especially close attention due to the exceptionally large transition dipole moments among Rydberg states, especially those belonging to the same n^* (which scales approximately $\propto n^{*2}$, where n^* is the effective principal quantum number). Large transition dipole moments make it possible to exert profound external influence over atoms or molecules even with relatively weak electric fields. Both the strength of the interaction with a static electric field (discussed in this paper) and the intensities of radiative transitions among Rydberg states are determined by the magnitude of the *same* transition dipole moment. Nevertheless, due to the complex patterns of multistate interactions among Rydberg states, high-resolution spectroscopic studies of the Stark effect in molecular Rydberg states have been limited to only a handful of cases. All of the molecules in which the Stark effect in Rydberg states has been studied have a molecular ion with either a small or zero permanent dipole moment. However, even in the absence of an external electric field the mechanism by which the dipole moment mixes the electron orbital angular momentum quantum number in Rydberg states differs profoundly from the mixing caused by the quadrupole moment and polarizabilities.

ℓ-mixing in molecular Rydberg states results from both the incomplete shielding of the ion core (also present in atoms), as well as the departure from spherical symmetry due to the presence of more than one nucleus (with ℓ being the orbital angular momentum for the Rydberg electron). For lower-ℓ states, core penetration of the Rydberg electron is the dominant cause of ℓ-mixing. For core-nonpenetrating states, ℓ-mixing caused by the ion core can be understood in terms of the static long-range properties of the ion core, such as multipole moments and polarizabilities. The interaction selection rules are such that the dipole field of the ion core causes interaction among states with ℓ differing by 1, while the quadrupole field of the ion core mixes states of ℓ differing by 2 or 0 (see Table I). In CaF, due to the large CaF^+ dipole and quadrupole moments, ℓ-mixing is profound. It is not limited only to s-d mixing, as in homonuclear molecules but affects all $\ell \leqslant 3$ states.[1]

In a nonrotating molecule the information about the different mechanisms of the interaction of the Rydberg electron with the ion core is not contaminated by rotation-electronic interactions. However, to be able to identify assignment-aiding patterns, spectra usually must be recorded from several rotational levels of an intermediate electronic state. Rotational assignments are then made by identifying pairs of spectral features (combination differences) with the same N

[a)]Electronic mail: rwfield@mit.edu.

TABLE I. Selection rules for interactions discussed in the text. Matrix elements for these types of interactions are nonzero when the conditions from the table are satisfied.

Interaction	$\Delta\ell$	ΔN^+	ΔN[a]
Ion-core dipole field operating on Rydberg electron	± 1[b]	± 1	0
Ion-core quadrupole field operating on Rydberg electron	0, ± 2[b]	0, ± 2	0
External homogeneous electric field operating on Rydberg electron	± 1	0	0, ± 1
External homogeneous electric field operating on the ion core	0	± 1	0, ± 1

[a]Electric field polarization can further affect these selection rules.
[b]These matrix elements are zero when $\Delta n^*=0$.

but different N' ($\mathbf{N}=\mathbf{J}-\mathbf{S}$; primed values pertain to the intermediate state, unprimed to a Rydberg state). As N increases, for a given N^+ value, the rotation-electronic interaction (ℓ-uncoupling) results in the evolution from Hund's coupling case (b) to Hund's case (d), and the intensity patterns expected for Hund's case (b) are distorted. As a result, combination differences in N become systematically unobservable. The distortion of the relative intensity patterns from those expected for Hund's case (b) to Hund's case (d) transitions can be understood in terms of the interference effects[2] (see Fig. 1). When the Rydberg state into which a transition is observed is not in the Hund's case (b) limit, we can decompose that state into Hund's case (b) basis states with different values of the Λ quantum number. The transformation between the Hund's case (b) $|\eta,\ell,\Lambda,N\rangle$ and Hund's case (d) $|\eta,\ell,N,N^+\rangle$ basis states is given by the following expression:

$$|\eta,\ell,\Lambda,N\rangle = \sum_{N^+} (-1)^{N^+-\ell+\Lambda}(2N^+ + 1)^{1/2}\begin{pmatrix} N & \ell & N^+ \\ \Lambda & -\Lambda & 0 \end{pmatrix} \times |\eta,\ell,N,N^+\rangle. \quad (1)$$

The low-n^* (and low-N') intermediate state through which the Rydberg state is accessed is usually in the Hund's case (a) or (b) limit and has a definite value of the Λ' quantum number. Since the final Rydberg state is Λ-mixed, transition amplitudes into $\Lambda=\Lambda'$ and $\Lambda=\Lambda'\pm 1$ basis states will interfere, resulting in the distortion of the relative intensity patterns of Hund's case (b) to Hund's case (b) transitions.

Analysis of the ℓ-uncoupling caused by the rotation-electronic interaction, $-B^+(\mathbf{N}^{\pm}\mathbf{L}^{\mp})$, in CaF is further complicated by strong ℓ-mixing caused by the nonsphericity of the ion core. Since the intermediate state used in our experiments on CaF is ℓ'-mixed, nonzero transition amplitudes into $\ell=\ell'\pm 1$ components (optically "bright") of the highly ℓ-mixed final Rydberg state will interfere as well. The effects of both ℓ-mixing and ℓ-uncoupling can result in the disappearance of one member, or a gross distortion, of the expected simple patterns in the spectrum. The distortion is especially strong for the lowest-N rotational levels, where the case (b) to (d) evolution is incomplete, and the rotational spreading of $N-1$, N, and $N+1$ levels, which is smaller than that at higher N, results in a higher density of spectral features around integer values of n^*, where the band origins for the core-nonpenetrating states are located.

We have previously described the use of polarization diagnostics to make N assignments even for the lowest-N rotational levels.[3] Here we perform a high-resolution analysis of the Stark effect in the spectrum of the CaF molecule, which has an ion core, CaF^+, with one of the largest permanent dipole moments known in a diatomic molecular ion, ≈ 9 D (Ref. 4) (origin at center of mass of CaF^+).

We describe several stages of the decoupling of the molecular Rydberg electron from the body frame caused by the external electric field. The weak-field Stark effect is employed to gain access to the f, g, and h states and to aid the assignment of the actual or nominal value of N^+, the rotational quantum number of the ion core ($\mathbf{N}^+=\mathbf{N}-\boldsymbol{\ell}$), for the lowest-$N$ rotational levels. From the analysis of the lowest-N rotational levels, we learn about the interactions of the core-nonpenetrating f, g, and h states with the lower-ℓ core-penetrating states.

Two models, based on the experimental data that cover the region surrounding $n^*=13$, have been developed previously to describe the Rydberg states of CaF. A global multichannel quantum defect theory (MQDT) model was used to fit the states from $n^*\approx 12-18$, $N=0-14$, $v^+=1$, $n^*\approx 9-10$, $N=0-14$, $v^+=2$, and $n^*\approx 7$, $N=3-10$, $v^+=3$ regions, and generated $0\leqslant\ell\leqslant 3$ quantum defect matrix and its derivatives with respect to the internuclear distance.[5] A complementary extended long-range model, which included the $3\leqslant\ell\leqslant 5$, $v^+=1$ states from the region of $13\leqslant n^*\leqslant 17$, yielded the values for dipole and quadrupole moments and the isotropic polarizability.[6] The interaction among $g(-4)$, $f(-3)$, and $d\,^2\Sigma^+$ states [here we use Hund's case (d) notation for the first two states: $\ell(\ell_R)$, where $\ell_R=N-N^+$ is the projection of ℓ on the ion-core rotational axis], as uncovered in the analysis of the lowest-N rotational levels presented in this paper, bridges the two models since in neither of the two previous models are all three of these states [$g(-4)$, $f(-3)$, and $d\,^2\Sigma^+$] present together. However, limitations in our fitting capabilities and the current dataset have prevented a global fit involving both sets of data.

II. BACKGROUND

In the Rydberg states of the hydrogen atom (see Ref. 7), an external homogeneous electric field mixes the states of opposite parity in steps of $\Delta\ell=\pm 1$, while m_j and m_ℓ are conserved (see Fig. 5 in Ref. 8). When Stark mixing between states that belong to the same n but different values of ℓ begins, higher-ℓ states gain a share of the bright character from the low-ℓ states, and a regular-appearing Stark manifold of higher-ℓ states appears in the spectrum. The energies of all features in the Stark manifold change linearly with the

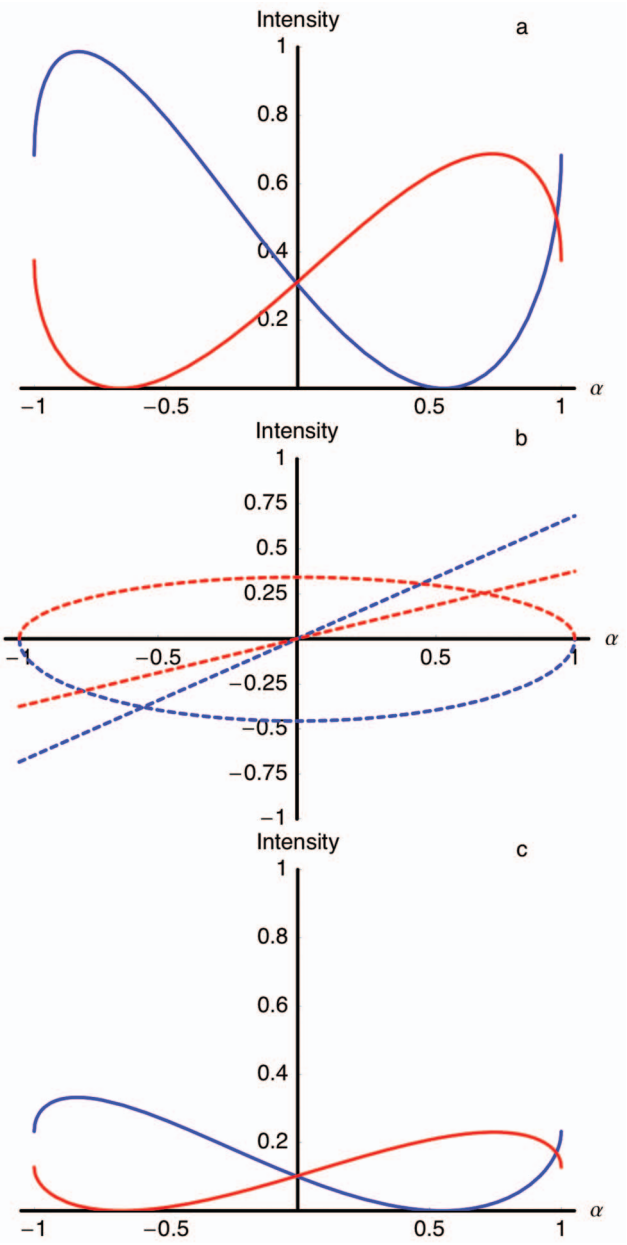

FIG. 1. Interference effects in the intensity of P (blue) and R (red) branches between a pure Hund's case (b) lower state, $N'=3$, and an upper state that is mixed in this basis. Plotted is the transition intensity (scaled to 1) as a function of the mixing coefficient, α. In (a) the transition is into the states $\alpha|f,\Sigma^+\rangle+\sqrt{1-\alpha^2}|f,\Pi^+\rangle$, from a lower state, $|d,\Sigma^+\rangle$. The plot for the case of the $\alpha|f,\Sigma^+\rangle-\sqrt{1-\alpha^2}|f,\Pi^+\rangle$ upper state is a mirror image of the plot in (a) with the y axis as the axis of reflection. Plot (a) is a square of the sum of Σ^+ and Π^+ contribution plotted in (b) for both P (blue) and R (red) transitions. Distortion of the pattern in (a) by ℓ-mixing is shown in (c). Here both states involved in the transition are ℓ-mixed in addition to being Λ-mixed, the lower state is $\eta|p\rangle-\sqrt{1-\eta^2}|d\rangle$ and the upper state is $\theta|d\rangle+\sqrt{1-\theta^2}|f\rangle$, with $\eta=0.5$ and $\theta=0.5$. Both (a) and (b) plots were produced using Eq. (5) from Ref. 3, but with a correction that $(1+\delta_{\Lambda',0}+\delta_{\Lambda,0}-2\delta_{\Lambda',0}\delta_{\Lambda,0})$ in that equation should appear with the exponent $1/2$ instead of $-1/2$. It was assumed that $S=0$, $J=N$, and $M_J=0$ in the plot. The intensities are scaled in the same manner as in (a). Since there are no Σ^- states in the CaF Rydberg supercomplex, there are no interferences in the Q branches excited from a Σ^+ intermediate state.

applied electric field. Once the field is increased above the Inglis–Teller limit, $E_{\text{Stark}}=1/3n^5$ a.u.,[7] members of Stark manifolds that belong to different values of n start to cross.

In atoms with one electron outside the closed shells (see Ref. 9, and specifically Fig. 7. therein), low-ℓ states penetrate more deeply into the ion core than the higher-ℓ states, and their energy is shifted away from the energy given by Rydberg formula for an integer value of n^*. When an external electric field is applied, the almost-degenerate higher-ℓ states mix at low field to form Stark manifolds similar to those in hydrogen, while the lower-ℓ states with larger quantum defects initially follow a second-order Stark tuning curve until they eventually merge with the high-ℓ Stark manifold of the same or neighboring n^* at higher field. One-electron alkali-like systems, unlike hydrogen, in addition show $\Delta n^*=\pm 1$ level mixing rather than level crossing above the Inglis–Teller limit, and a series of avoided crossings is formed. In both hydrogen atom and alkali atoms, destruction of zero-field quantum numbers proceeds in two stages. In the first stage the electric field destroys ℓ (which gets decoupled from electron spin s) and therefore destroys j. In the second stage, the principal quantum number (n or n^*) ceases to be a good quantum number.

The structure of molecular Rydberg spectra is richer than that of atomic Rydberg spectra due to the vibrational and rotational degrees of freedom, as well as the vibrationally or rotationally modulated anisotropy of the ion core. Core-penetrating states, similar to the atomic case, have nonzero quantum defects, while the core-nonpenetrating states cluster near integer values of n^*. However, because of the vibrational and rotational structure, each rotation-vibration state of the ion core will have a series of Rydberg states converging to it. Each series, associated with a different ionization limit, is characterized by the vibrational and rotational quantum numbers for the ion core, v^+ and N^+, respectively.

For atomic hydrogenic Rydberg states, transition dipole moments among the states that belong to the same n but differ in ℓ by 1, scale as $\langle n,l|er|n,l+1\rangle=-3/2ea_0n\sqrt{n^2-\ell^2}$ (Ref. 7) and even at intermediate values of n, are exceptionally large compared to the typical permanent molecular dipole moments (see Fig. 2). The hydrogenic transition dipole moment for $13g\leftarrow 13f$ is $\approx$600 D, compared to $\approx$9 D, the permanent dipole moment for CaF^+. The selection rules for the Stark matrix elements, where the external homogeneous electric field interacts with these large intracomplex Rydberg–Rydberg transition dipole moments, are such that the quantum numbers for the Rydberg electron are mixed by the field ($\Delta\ell=\pm 1$, $\Delta N=0,\pm 1$), but those for the ion core are conserved ($\Delta N^+=0$, $\Delta v^+=0$) (see Table I). Because of the much larger size of the intracomplex Rydberg–Rydberg transition dipole moment relative to the permanent ion-core dipole moment, in the absence of accidental degeneracies among states with different N^+ values, a weak external electric field mixes ℓ and N for the Rydberg electron, but N^+-mixing only becomes appreciable at much higher field strengths. Thus the first stage of the interaction with the external homogeneous electric field can be observed in isolation. While in atoms the destruction of zero-field quantum numbers by the external electric field proceeds in only two stages (mixing of ℓ and mixing of n), the Stark-induced mixing process in molecular Rydberg states exhibits several additional stages. In CaF, for example, ℓ, N, N^+, n^*, and v^+ are

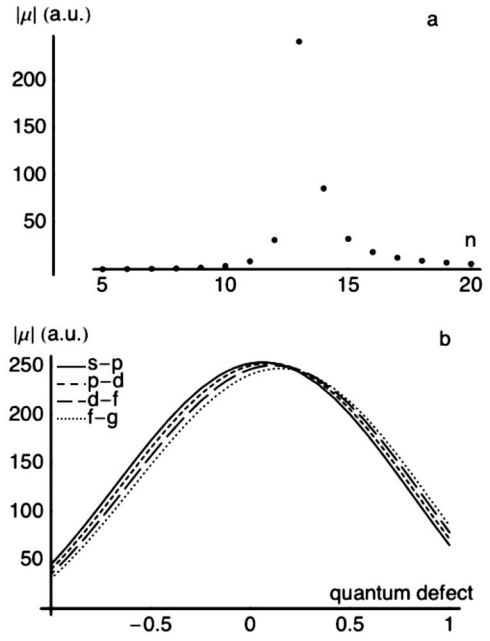

FIG. 2. Transition dipole moments for which ℓ of the Rydberg electron changes by ± 1, in a.u. Part (a) gives the variation in the $\langle n'=13,\ \ell'=3|\mu|n,\ \ell=4\rangle$ transition dipole moment with n, calculated using hydrogenic wavefunctions (for integer values of n). (b) displays the dependence of the intracomplex (same-n^*) transition dipole moments on the quantum defect, δ, for the $\langle n^{*\prime}=13,\ \ell'=0,1,2,3|\mu|n^*=n^{*\prime}+\delta,\ \ell=\ell'+1\rangle$ transition moment, where δ varies between -1 and 1. Nonhydrogenic dipole moments were evaluated using the method described in Ref. 38.

sequentially destroyed by the electric field. We study, in detail, the first stage of destruction in which ℓ and N are mixed.

How well the different decoupling stages are separated as the electric field is increased depends on the strength of the electric field, the n^* region in which the observations are made, and the values of molecular parameters. These molecular parameters include rotational and vibrational constants and the quantum defects (dependent on the internuclear distance, multipole moments, and polarizabilities). For CaF at $n^*=13$, which we studied, it is possible to observe the different stages of Stark decoupling associated with the N^+-rotational structure but not those due to the vibrational structure. When the electric field is applied, core-nonpenetrating states mix first because of their near degeneracy. ℓ ceases to be a good quantum number, and N is destroyed along the way. N^+ is approximately conserved at this stage. Stark manifolds associated with each value of the N^+ quantum number are formed, and manifolds associated with values of N^+ with optically bright character appear in the spectrum. This is a consequence of the intermediate state being N^+-mixed since it is not in the Hund's case (d) but the Hund's case (b) limit. The existence of several Stark manifolds (associated with different values of N^+) is the main difference from the Stark effect in atomic Rydberg states.

As the electric field increases, either N^+ is destroyed, or some low-ℓ penetrating states join the high-ℓ Stark manifold first since some of the core-penetrating states are accidentally located in the proximity of an integer value of n^*. Mixing of N^+ initially occurs indirectly as a consequence of the rotation-electronic and field-induced interaction among the ion-core mixed states. Eventually, the electric field is expected to mix the states that belong to different N^+ clusters directly, through interaction with the permanent dipole moment of the ion core, to form a hydrogenic Stark manifold associated with a particular n^* and v^+. N^+-mixing due to the permanent dipole moment of the ion core was not investigated in this paper and was neglected in our effective Hamiltonian model (Sec. IV).

The effect of an external electric field on both the structure and dynamics of molecular Rydberg states has previously been studied experimentally, and different theoretical descriptions have been developed. In addition to studies at very high n^*, in the context of ZEKE photoelectron spectroscopy experiments, various aspects of the Stark effect have been studied at intermediate n^* in H_2,[10–17] NO,[18–23] Na_2,[24–27] H_3,[28,29] and Li_2.[30,31] Unlike these systems, CaF^+ possesses a large dipole moment, which causes profound mixing among the $\ell \leqslant 3$ states. It presents an ideal testbed for studying the competition between the mixing caused by the external and internal electric fields. Modeling of the Stark effect in molecular Rydberg states usually relies on an adaptation of MQDT to include Stark interactions[12,18,19,25,26] or effective Hamiltonian matrix diagonalization techniques.[10,15,18,28,29] When the interaction with the states that belong to a neighboring n^* value is weak, as is the case at lowest-N core-nonpenetrating states in zero or low external electric field, the H_{eff} matrix diagonalization method can provide an adequate description.[18]

Even though spectral congestion in the already complex spectra of Rydberg states increases when an external electric field is applied, the emergence of Stark manifolds has previously been used for diagnostic purposes.[32] In Ref. 32, core-penetrating and core-nonpenetrating states in H_2 could be experimentally distinguished when an external electric field is applied. In spectra recorded from an intermediate d state, an optically bright core-nonpenetrating f state is located in the vicinity of the higher-ℓ cluster, and applying the electric field mixes some bright f character into the higher-ℓ states of the Stark manifold. In contrast, an optically bright core-penetrating p state at the same field strength and similar n^* value has no neighboring states with which it can be forced by the Stark field to interact. In addition to distinguishing between field-non-mixed core-penetrating states and the strongly field-mixed core-nonpenetrating states, a weak electric field can also be used for diagnostic purposes. We applied a weak electric field (<100 V/cm) to access states of higher $\ell(\ell \geqslant 3)$, which are usually not accessible directly, and to make (or verify) assignments of actual or nominal value of N^+. In addition, since the Stark effect mixes states of opposite parities, transitions into N states that are dark at zero field appear when the electric field is applied. This ability to observe a particular state from several values of N' is helpful in verifying and extending the zero-field assignments. Assignments made by this method are especially useful for the lowest-N rotational levels, where the combination differences are often systematically unobservable, as described in Sec. I. However, the lowest-N rotational levels are of greatest value for disentangling the short-range and long-range interactions of the Rydberg electron with the ion core.[3]

The lowest-N levels encode the information free from distortion by the rotation-electronic coupling. In this paper we describe the application of the Stark effect to access and assign the actual or nominal value of N^+ quantum number of, the lowest-N rotational levels of f, g, and h states, and we characterize the mixing of the core-nonpenetrating states with the core-penetrating states.

Modeling of the Stark effect in Rydberg states requires knowledge on the zero-field quantum defects. We have exploited the extended long-range model[6] to provide a zero-field description of the core-nonpenetrating states. Based on observation of the lowest-N rotational states, we have determined the core-penetrating characters admixed into the f, g, and h states and, by comparing the experimentally observed Stark effect patterns to the calculated ones, we show that our extended long-range model is valid for higher-ℓ states, which had not been explicitly fitted in our determination of the long-range parameters and which first appear in the spectrum only when the electric field is applied.

III. EXPERIMENT

Our molecular beam double resonance excitation scheme has been described elsewhere[3] and only the aspects of the experiment pertaining to excitation in the presence of the external electric field (further referred to as E_{Stark}) will be given here. Excitation of CaF molecules by two almost collinear laser pulses occurs between metal meshes P_l and P_u, parallel to each other and separated by 1 cm (modification of the R. M. Jordan Co. C-677 model). In the experiment at $E_{\mathrm{Stark}}=0$, both P_l and P_u were held at the same potential during the excitation (1500 V). The propagation direction of the laser pulses, the direction of the molecular beam, and the direction of E_{Stark} were mutually perpendicular. In the experiment discussed here, the molecules were excited into an autoionizing state, which is a member of a Rydberg series converging to the $v^+=1$ ionization limit. 200 ns after the excitation, an additional 200 V/cm positive potential (extraction pulse) was applied to P_l to repel the ions formed by autoionization toward the time-of-flight mass spectrometer. Ions are then detected at a multichannel plate detector. The electric field applied to P_l and P_u is controllable to ± 1 V/cm in our current arrangement. No attempt was made to characterize the stray fields, or the field inhomogeneity, but in the spectral region studied here ($n^*=13$) electric fields of the order of several volts have a negligible effect compared to the 0.1 cm^{-1} resolution of our current experiment.

In the experiment with nonzero E_{Stark}, the P_l plate was held at a different potential (1500 V$+E_{\mathrm{Stark}}\times 1$ cm) than the P_u plate (1500 V) during the optical excitation pulses. The range of the values of the applied E_{Stark} field was 40–180 V/cm (varied in steps of 10), and 300 V/cm (in addition to the zero-field conditions described previously). At E_{Stark} smaller than 40 V/cm, very small changes were observed in the spectrum, and this region of electric field strengths was not systematically studied. In the experiments performed in the presence of the electric field, E_{Stark} affects the arrival times of the ions, as well as the spread of the arrival times at the detector. Whenever it was necessary, adjustments were made to the ion-optics focusing fields to compensate for this distortion of the signal. No attempt was made to normalize the relative intensities of the spectra recorded at different values of E_{Stark}.

Under these conditions, we recorded double resonance spectra in the energy region around the integer value of $n^*=13$ for the N' values of 0, 1, 2, and 3 in the $F'\,^2\Sigma^+$ intermediate state [accessed by $P(1)$, $R(0)$, $R(1)$, and $R(2)$ pump transitions from the ground $X\,^2\Sigma^+$ state]. In our excitation scheme, the spin fine structure doublets are not resolved in the intermediate state, and neither spin fine structure nor spin-orbit structure are resolved in the Rydberg states in this n^* region. All CaF spectra were calibrated to 0.1 cm^{-1} using high-temperature iodine spectra ($\approx 100\,^\circ$C) recorded simultaneously (an extracavity etalon was not used).

Although, in all of the spectra recorded for the purpose of making the assignments, the polarization arrangement was pp, the effect of the polarization arrangement on the appearance of the Stark spectrum was examined in a subset of spectra by additionally recording spectra in ps, sp, ss, RHCP-RHCP-vertical, and RHCP-LHCP-vertical polarization arrangements [p and s denote polarization parallel and perpendicular to the direction of the Stark field, respectively, while RHCP and LHCP are right and left hand circularly polarized photons, respectively; the ordering specifies pump photon–probe photon (–Stark field), respectively]. The two circularly polarized photons have components in the direction of the Stark field vector, and it is more convenient to analyze this particular polarization arrangement in a coordinate system in which the quantization axis z is selected to lie along the direction of the propagation of the laser pulses, and x axis is selected to be in the direction of the Stark field. Then the selection rules are $\Delta M_J=\pm 1$ for the Stark field, $\Delta M_J=1$ for the RHCP photon, and $\Delta M_J=-1$ for a LHCP photon. For the experimental arrangement in which both photons are linearly polarized, it is more convenient to use the standard coordinate system with the quantization axis z being along the direction of the Stark field. The selection rules are $\Delta M_J=0$ for the Stark field, as well as for both photons. Some of the spectra used for monitoring the polarization dependence were recorded at electric field strengths larger than those specified in the previous paragraph (E_{Stark} up to 350 V/cm).

IV. CALCULATION

To model the experimentally observed results, an effective Hamiltonian was set up. The calculation was done in the energy region around $n^*=13$ and, since the range of the electric field strengths studied was well below the Inglis–Teller limit ($\approx$4.6 kV/cm for this n^*), we did not include interactions with the states from the neighboring n^*. Even in $n^*=13$, only the core-penetrating states that are in the neighborhood of integer n^* ($13.19\Sigma^+$, $12.98\Pi^\pm$, $13.14\Delta^\pm$, and $12.88\Sigma^+$) were included in our calculation, in addition to all of the core-nonpenetrating states ($3\leqslant\ell\leqslant 12$).

The Hamiltonian in the absence of the electric field is given by

$$H_0 = H_{\rm el} + H_{\rm rot} + H_{SO}, \tag{2}$$

where, since we did not consider v^+-changing interactions, the vibrational Hamiltonian is implicitly included in the electronic term by using the ionization potential for $v^+=1$ and $N^+=0$. We determine the energies of the rotationless core-penetrating states by a fit. Core-penetrating states are well described by Hund's case (b), and we use the case (b) basis in order to implement the fitting procedure. In the Hund's case (b) basis it is straightforward to add (or remove) core-penetrating states to the basis set one by one, which is why the Hund's case (b) basis was preferred in our fitting procedure relative to the Hund's case (d) basis, which is commonly used to describe Rydberg states, especially in the presence of a field.

For core-nonpenetrating states, the $H_{\rm el}$ was calculated using Watson's long-range expression,[33] corrected for the polarizability terms.[6] This approximate expression contains only diagonal matrix elements,

$$H_{\rm el} = {\rm IP}_{v^+=1} - \frac{R}{n^2} + \frac{2(\mu^2 - Q)(\ell(\ell+1) - 3\Lambda^2)}{n^3(2\ell+1)(2\ell+3)(2\ell-1)\ell(\ell+1)} + \alpha\frac{2(\ell(\ell+1) - 3n^2)}{n^5(2\ell+3)(2\ell+1)(2\ell-1)\ell(\ell+1)} + \gamma\frac{4(\ell(\ell+1) - 3n^2)(\ell(\ell+1) - 3\Lambda^2)}{3n^5(2\ell+3)^2(2\ell+1)(2\ell-1)^2\ell(\ell+1)}, \tag{3}$$

where ${\rm IP}_{v^+=1}=47\,686\ {\rm cm}^{-1}$ is the ionization potential for $v^+=1$ (Ref. 34) and $n=13$ in the region studied here. μ and Q are the permanent dipole and quadrupole moments of the CaF^+ ion, respectively. The value of μ^2-Q was previously determined by fits[1] and we used 11.3 a.u. α is the isotropic polarizability, and we used the value of 15 a.u. previously determined by a fit.[6] γ is the anisotropic polarizability, the value of which is difficult to determine by the fit when the separation of the long-range from short-range interactions is incomplete, and we used the value of 5 a.u.[6]

For the core-penetrating states, the value of the matrix elements of $H_{\rm el}$ were determined by fit rather than from the long-range interaction terms, as described below.

The rotational Hamiltonian is given by

$$H_{\rm rot} = \sum_{\ell} c_{\ell}^{\ell_1,\Lambda} c_{\ell}^{\ell_2,\Lambda} B^+[N(N+1) + \ell(\ell+1) - 2\Lambda^2] \tag{4}$$

for $\Delta\Lambda=0$ and by

$$H_{\rm rot} = -\sqrt{1 + \delta_{\Lambda_1,0} + \delta_{\Lambda_2,0}}\sum_{\ell} c_{\ell}^{\ell_1,\Lambda_1} c_{\ell}^{\ell_2,\Lambda_2} B^+ \times\sqrt{N(N+1) - \Lambda_1\Lambda_2}\sqrt{\ell(\ell+1) - \Lambda_1\Lambda_2} \tag{5}$$

for $\Delta\Lambda=\pm 1$. $B^+=0.37\ {\rm cm}^{-1}$ is the rotational constant of the CaF^+ ion.[1] The $c_{\ell'}^{\ell,\Lambda}$ are the elements of the eigenvector decomposition (admixed ℓ'-amplitude of a nominally $|\ell,\Lambda\rangle$ state).

The degeneracy between states of the same N but different J was removed by adding a small spin-orbit splitting

$$\Delta E = E(N+1/2) - E(N-1/2) \approx \frac{A\Lambda^2}{N}\left[1 - \frac{A\Lambda^2}{2B}\right] \tag{6}$$

with $A=0.01\ {\rm cm}^{-1}$. The splitting is smaller than our experimental resolution, but removing this degeneracy suppressed nonphysical eigenvalues, which resulted from diagonalizing a large-size matrix containing multiple pairs of degenerate entries.

Diagonalization of the Hamiltonian was performed in MATHEMATICA. In the absence of an external electric field, the values of some of the $c_{\ell'}^{\ell,\Lambda}$ were varied until agreement between the calculated and the experimentally observed energy values was obtained. In addition, the values of the diagonal matrix elements of $H_{\rm el}$ for the core-penetrating states were varied as well. The comparison between the calculated and the experimentally observed energies was made for a subset of the experimentally observed core-penetrating and core-nonpenetrating states with $0\leqslant N\leqslant 6$ in $n^*=13$. The fit parameters were varied by hand and the correct matching between the corresponding calculated and observed states was ensured by inspection. In rare instances in which the algorithm for matching the states failed, the state for which the disagreement occurred was removed from the comparison. The sets of computed states of positive and negative Kronig symmetry[35] were compared to the experimental data independent of each other. The fit parameters were varied until the standard deviation in the region of the comparison became smaller than $0.2\ {\rm cm}^{-1}$. In order to speed up the convergence, as initial values for the $c_{\ell'}^{\ell,\Lambda=0}$ (ℓ is nominal and ℓ' admixed character), we used a previously available, but unpublished, set of *ab initio* eigenvector decomposition coefficients calculated as in Refs. 4 and 36. For $c_{\ell'}^{\ell,\Lambda=0}$, mixing of the states with $\ell\leqslant 5$ was considered. Our fit was not sensitive to small mixing coefficients for $c_{\ell'}^{\ell,\Lambda=1}$ and $c_{\ell'}^{\ell,\Lambda=2}$ when $\ell>3$, and we were only able to determine the mixing coefficients for the $^2\Sigma^+$ states ($\Lambda=0$). For $c_{\ell'}^{\ell,\Lambda=1}$, only small adjustments were made to the values presented in Ref. 5, and no mixing with $\ell>3$ states was included. For $c_{\ell'}^{\ell,\Lambda=2}$ we used the values given in Ref. 5, and no mixing with $\ell>3$ states was included. We attempted varying $c_{\ell'}^{\ell,\Lambda=1,2}$ and including the $\ell=4$ states, but our fit was not sensitive to these variations. Variation in coefficients for $c_{\ell'}^{\ell,\Lambda>2}$ was not attempted. The coefficients that were not varied were set to $\delta_{\ell,\ell'}$. Since the zero-field Hamiltonian is block diagonal in the Kronig symmetry, the parameters were varied independently in + and − Kronig symmetry blocks. This approach is justified, in part, by the fact that states belonging to higher values of v^+ were not included in the calculation. Higher v^+ interlopers affect the states of positive and negative Kronig symmetry in different ways.[1,5] Small variations in α, γ, and μ^2-Q were attempted, but the best agreement between the calculated and the experimentally observed energy values was observed for

the values previously reported.[1,6]

Once agreement between experiment and calculation at zero field was optimized, interactions due to the external electric field were included in the Hamiltonian. We made the assumption that, for the range of the electric field strengths used here, N^+-changing interactions are negligible. When only the ℓ-changing interaction is considered, the Stark matrix element for the electric field oriented along the z axis is given by (the derivation of this expression will be discussed elsewhere; $e=1$ a.u.):

$$H_{\mathrm{Stark}} = eE_{\mathrm{Stark}} \sum_{\ell_1,\ell_2} c_{\ell_1}^{\ell',\Lambda_1} c_{\ell_2}^{\ell'',\Lambda_2} (-1)^{N_1+N_2+1/2+M_J} \left(\frac{1+(-1)^{p_1+p_2+1}}{2} \right) \langle n,\ell_2|r|n,\ell_1\rangle$$
$$\times \sqrt{1+\delta_{\Lambda_1,0}+\delta_{\Lambda_2,0}-2\delta_{\Lambda_1,0}\delta_{\Lambda_2,0}} \sqrt{(2N_1+1)(2N_2+1)(2\ell_1+1)(2\ell_2+1)(2J_1+1)(2J_2+1)}$$
$$\times \begin{pmatrix} \ell_2 & 1 & \ell_1 \\ 0 & 0 & 0 \end{pmatrix} \begin{pmatrix} N_1 & N_2 & 1 \\ -\Lambda_1 & \Lambda_2 & \Lambda_1-\Lambda_2 \end{pmatrix} \begin{pmatrix} \ell_2 & \ell_1 & 1 \\ -\Lambda_2 & \Lambda_1 & \Lambda_2-\Lambda_1 \end{pmatrix} \begin{pmatrix} 1 & J_1 & J_2 \\ 0 & -M_J & M_J \end{pmatrix} \begin{Bmatrix} 1 & J_1 & J_2 \\ \frac{1}{2} & N_2 & N_1 \end{Bmatrix}. \quad (7)$$

Transition dipole moments were calculated by numerical integration of hydrogenic wavefunctions. Hydrogenic dipole moments are a good approximation for the core-nonpenetrating states; however, it is likely that the calculated relative intensities were affected by this approximation for transitions between the core-penetrating and core-nonpenetrating states. Since the comparison with experiment was done at low electric field strength and low N (the states accessed through $N'=0$, 1, 2, and 3 intermediate state levels), values of $N \leqslant 10$ were considered sufficient for the calculation in the presence of the electric field. The total Hamiltonian, when the external electric field is along the z axis,

$$H = H_0 + H_{\mathrm{Stark}} \quad (8)$$

was diagonalized for values of the electric field strength ranging between 0 and 180 V/cm, in steps of 10 V/cm. The Hamiltonian is block diagonal in M_J, so all M_J values accessible in the experiment were treated independently.

In order to compare the calculation to the experiment, a spectrum was calculated from the energy values and eigenvectors obtained by the diagonalization, and convoluted with 0.1 cm^{-1} Lorentzian line shapes. The eigenvectors were used to calculate the transition intensities in the double resonance experiment using the expressions for transition intensities among Hund's case (b) states given in Ref. 3 with the correction that $(1+\delta_{\Lambda',0}+\delta_{\Lambda,0}-2\delta_{\Lambda',0}\delta_{\Lambda,0})$ should appear with the exponent $1/2$ instead of $-1/2$. Since the calculation is done for the lowest-N rotational levels, we do not neglect the difference between J and N when calculating the transition intensities. The spectrum was calculated for the pp polarization arrangement.

A simplifying assumption was made for the ℓ character of the intermediate $F'\,^2\Sigma^+$ state. It was assumed that this state is composed exclusively of p and d characters in order to avoid having to consider interferences among different transition amplitudes into the Rydberg states (for example, had f character been included in the intermediate state, then the $d \leftarrow p$ and $d \leftarrow f$ transition amplitudes into each Rydberg state would interfere). Similarly, an assumption was made for the ground $^2\Sigma^+$ state ℓ-characters (to be only s-p- mixed). No attempt was made to determine the ℓ character of the ground and intermediate states. Instead, since with our assumptions there is no interference between two basis-state transition paths, the intensity of the $f \leftarrow d \leftarrow p$ transition path relative to that of the $d \leftarrow p \leftarrow s$ transition path was adjusted by varying only one parameter by hand to get the best agreement with the experimentally observed intensity distribution.

V. RESULTS AND DISCUSSION

A. Stages of decoupling

In the absence of an external electric field, the most suitable representation for a molecular core-nonpenetrating Rydberg state is the Hund's case (d) basis. Each ℓ state is split into $2\min(N,\ell)+1$ components with different value of $\ell_R(\ell_R=N-N^+)$ due to the coupling of ℓ and $\mathbf{N}^+(\mathbf{N}=\boldsymbol{\ell}+\mathbf{N}^+)$. Each of the ℓ_R components, for a fixed N, will have a different value of N^+. When Hund's case (d) is the appropriate coupling case, the energy-level pattern-forming quantum number in the spectrum is N^+, and the states with different values of the quantum number N belonging to the same value of N^+ cluster together in energy.

In the presence of the electric field, interaction among some of the previously uncoupled states is turned on. The Stark effect in molecular Rydberg states has its origin either in the permanent dipole moment of the ion core or the transition dipole moment. For two Rydberg states belonging to the same-n^* supercomplex, the transition dipole moment is usually orders of magnitude larger than the permanent dipole moment of the ion core even for a highly dipolar ion such as CaF^+. When n^* is sufficiently large, the dominant interaction with the external electric field will thus come from intracomplex $(\Delta n^* < 1)$ transition dipole moments. The leading term in the Stark Hamiltonian is given by Eq. (7). Selection rules for this type of interaction are $\Delta\ell = \pm 1$, $\Delta N = 0, \pm 1$, and $\Delta N^+ = 0$ (see Table I), and the interaction occurs exclusively within a particular N^+ -cluster. The number of states that

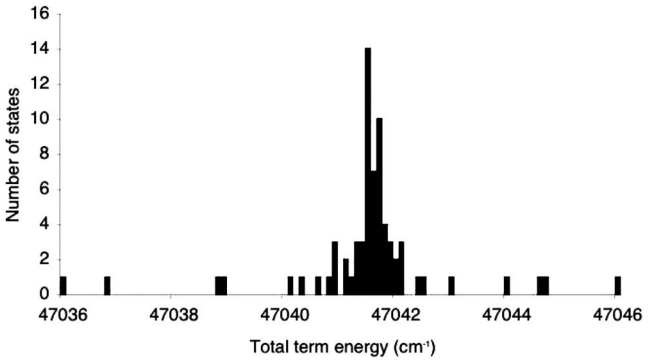

FIG. 3. Calculated or experimentally observed (where available) energies of all of the core-nonpenetrating ($3 \leqslant \ell \leqslant 12$) states that belong to the $N^+=3$ cluster in $n^*=13$. Most of the states are located near the center of the cluster, especially at higher values of ℓ and N. Outliers are found among lower-ℓ, lower-N states for which the evolution toward Hund's case (d) is not complete, or where core-penetration effects are non-negligible.

belong to a particular N^+ -cluster, among which mixing due to the dominant term in the CaF Stark Hamiltonian can occur, is

$$\sum_{\ell=3}^{n-1} \sum_{N=N^+-\ell}^{N^++\ell} (2\min(\ell,N)+1). \tag{9}$$

The zero-field structure within a particular N^+ cluster is such that states with higher values of N and ℓ quantum numbers are clustered more closely together in energy [the evolution toward Hund's case (d) is complete], while the outliers in energy within the same N^+ cluster are found among the lower-N, lower-ℓ states, where the evolution toward Hund's case (d) is less complete (see Fig. 3). With the resolution available in our experiment, only these low-N, lower-ℓ (f, g, and sometimes h) outliers are sufficiently separated from the high density of states at the center of the cluster to be assigned. These states contain the most information about the interaction of the core-nonpenetrating states with the core-penetrating states. Because of their low-N character, these outliers will be experimentally accessible when the spectrum is recorded from the lowest-N rotational levels in the intermediate state. In addition, the number of ℓ_R components present at low N is smaller than at high N. Thus selecting low N in the intermediate state helps reduce the number of states accessed at zero field and the number of states that share the bright character at the lowest Stark fields, and low N provides access to the states most useful in analyzing the interaction with the core-penetrating states.

The appearance of a molecular Rydberg Stark spectrum in a particular n^* (see Fig. 4) is determined by the amplitudes of ℓ-changing Stark interaction and N^+ -changing Stark interaction relative to the zero-field energy splitting caused by multipole moments, polarizabilities, and rotation. In weak electric fields, unless there is an accidental degeneracy among the states with neighboring N^+ values, the mixing first starts to occur among the states with ℓ differing by ± 1, but having the same N^+. It is only as the field strength increases that the mixing of states belonging to different N^+ complexes starts to occur. In the case of CaF, a manifold of states having different ℓ but the same n^* and the same N^+ starts to appear

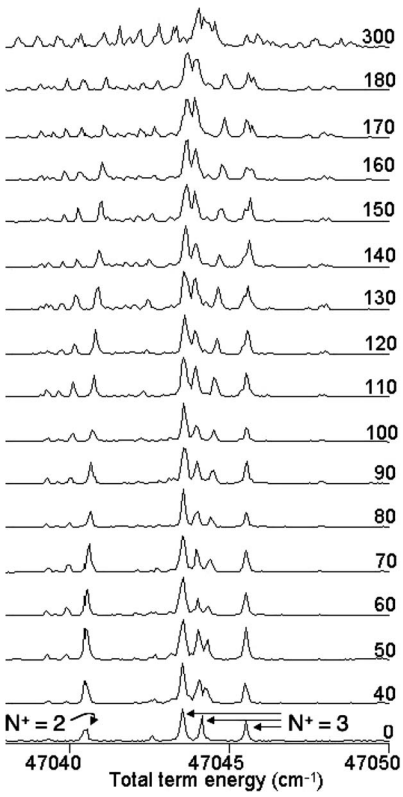

FIG. 4. Stark effect in the energy region around the integer value of $n^*=13$, experimentally observed in double resonance spectra from the $N'=1$ intermediate state, in the *pp* polarization arrangement. A weak electric field causes the Stark manifolds associated with different values of N^+ to appear, but as the field increases, these manifolds overlap and, owing to Stark interactions among them, are expected to merge when the field increases sufficiently. The electric field in V/cm is given on the right hand side of the plot. The N^+ values of the dominant zero-field bright features are marked on the plot.

around each N^+ that is accessible for a particular choice of pump transition. The relative intensities of each of these N^+ -manifolds will differ from one N^+ value to the next. As the electric field increases, states belonging to two different N^+ -clusters start to overlap and are expected to interact when the external field increases sufficiently (see Fig. 4).

B. Effective Hamiltonian matrix diagonalization

The region of $n^*=13$ has previously been studied and most of the $\ell \leqslant 3$ and some of the $\ell > 3$ states have been assigned for the values of the rotational quantum number N up to 12.[1,6] However, most of the rotational assignments for the lowest rotational levels of the core-nonpenetrating states were not previously available. Due to the opposing effects of ℓ-mixing and ℓ-uncoupling, spectral patterns are complex and rotational assignments are problematic, especially for the lowest rotational levels. Assignments additional to those published in Refs. 1 and 6 have been made using polarization diagnostics described in Ref. 3. Good agreement between the fit described in Sec. IV and the experimentally observed spectra was critically dependent on correct assignments of the lowest rotational levels at zero field. These low-N assignments were also a *sine qua non* to making new assignments in the presence of the electric field.

TABLE II. Best fit values for the ℓ mixing coefficients of rotationless p, d, f, g, and $h\ ^2\Sigma^+$ states. The $s\ ^2\Sigma^+$ basis state was not included in the fit, as it was not located near an integer value of n^*. Its ℓ-decomposition corresponds to that of Ref. 5. Nonunity in the sum of *squared* mixing coefficients is due to the loss of $v^+=1$ basis state character due to coupling with higher-v^+ states.

State	s	p	d	f	g	h	Sum
$12.88\ ^2\Sigma^+$	−0.593	−0.805	0.018	0.013	−0.004	0	1.00
$13.19\ ^2\Sigma^+$	0.135	−0.142	0.903	−0.365	0.111	0.026	1.00
$f\ ^2\Sigma^+$	−0.009	0.117	−0.295	−0.821	0.378	−0.093	0.93
$g\ ^2\Sigma^+$	0	−0.017	−0.181	−0.329	−0.850	0.369	1.00
$h\ ^2\Sigma^+$	−0.006	−0.060	−0.161	0.125	0.327	0.921	1.00

The standard deviation between the fit and the experiment was $<0.2\ \mathrm{cm}^{-1}$. The coefficients in the eigenvector decomposition, for $\Lambda=0$ states and ℓ ranging from 0 to 5, that gave the best agreement between the fit and the experiment are given in Table II. Of the core-penetrating states included in the fit, the $13.19^2\Sigma^+$ state was found to be most strongly mixed with the core-nonpenetrating states. Including the $12.88^2\Sigma^+$ state did not significantly affect the fit. Mixing with states with ℓ higher than 5 was not included in the fit since states with $\ell>5$ have not been experimentally observed at zero field. Only $v^+=1$ states were included in the fit, although interactions with the $v^+>1$ interlopers have been described.[5] A small deviation from unity of the sum of squared mixing coefficients for a particular ℓ was allowed in order to allow for the losses of ℓ-character due to coupling with states of higher v^+. Because of the exclusion of mixing with $\ell>5$ states, it is possible that the mixing coefficients for $h(\ell=5)$ states are affected by "edge effects" that result from this ℓ-cutoff. Since our fit was not sensitive to the variation of $c_{\ell'}^{\ell,\Lambda=1}$ and $c_{\ell'}^{\ell,\Lambda=2}$, values from Ref. 5 were used, with only a minor modification in the case of $\Lambda=1$.

The mixing coefficients in Table II indicate a nonnegligible core-penetrating character of the $g(-4)$ state [Hund's case (d) notation, denoting $\ell(\ell_R)$, where ℓ_R is the projection of ℓ on the rotational axis of the ion]. The strong interactions among the core-nonpenetrating $g(-4)$ and $f(-3)$ states, and a core-penetrating $13.19^2\Sigma^+$ state, are reflected by the mixing coefficients in Table II. Neither of the two models developed previously to describe the Rydberg states of CaF in this n^* region includes all three of the states found to interact strongly in this analysis. The interaction of the core-penetrating states ($\ell=0$, 1, and 2) with the partially penetrating f states in CaF has previously been modeled using an MQDT fit.[34] That fit has been extended by the addition of higher-v^+ interlopers.[5] On the other hand, core-nonpenetrating f, g, and h states, accessed predominantly at intermediate N and $13\leqslant n^*\leqslant 17$ of CaF, have been fitted to a long-range model.[6]

The interactions among $g(-4)$, $f(-3)$, and $13.19^2\Sigma^+$ states are also obvious from the energy and intensity patterns in the observed spectra, plotted in Fig. 5. Even though it is impossible to model these three states in isolation from other Rydberg states in their vicinity, it is still obvious that there is a strong interaction among all three of them. The polarization dependence of the transition intensity confirms that all three states involved in this interaction have the same N value. The usefulness of lower-N rotational assignments in the separation of the short-range and long-range interactions is evident in Fig. 5. It is only in the several lowest values of N that the strong three-state interaction becomes obvious, while, if only $N>4$ assignments are considered, this interaction remains too weak to be detected. Our previous fit, described in Ref. 6, gave nonphysical values for the anisotropic polarizability because the interaction with core-penetrating states was incompletely removed from our long-range model.

Using the coefficients given in Table II, we produced spectra by the method described in Sec. IV. Figure 6 displays the calculated and observed spectra recorded from the $N=3$ level in the intermediate state for electric field strengths of 0, 60, 120, and 180 V/cm. Within one spectrum, the quality of agreement between the calculated and the experimentally observed transition intensities varied from one N^+ cluster to another. We assumed that the intermediate state is a pure-Λ state, but ℓ-mixed. A pure-Λ, pure-ℓ state in a Hund's case (b) basis, when decomposed in a Hund's case (d) basis, spans either all-even or all-odd N^+ -basis states. However, a pure-Λ but mixed-ℓ state spans both even and odd values of N^+. However, since we assumed that the intermediate state contains *only* p and d characters, this limits the different N^+

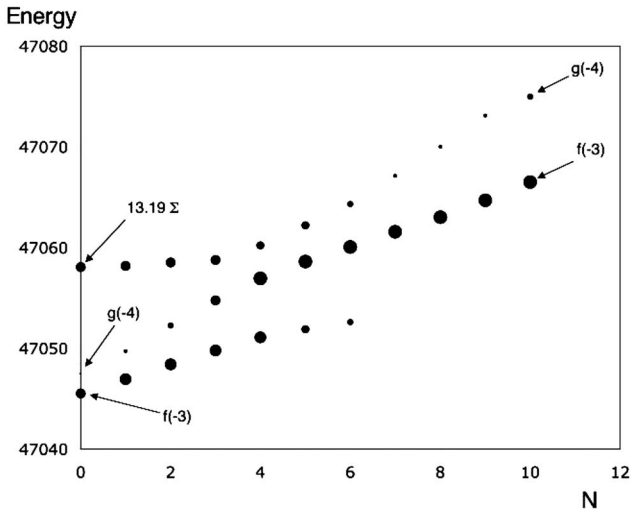

FIG. 5. Interaction among $f(-3)$, $g(-4)$, and $13.19\ ^2\Sigma^+$ states. The $\ell(\ell_R)$ labels at high N correspond to the assignments in Ref. 6. Marker sizes approximately represent the experimentally observed intensities of the spectral features. The interactions among these three states become apparent only for $N\leqslant 4$ rotational levels, and could remain unnoticed if the lowest-N rotational assignments are not available.

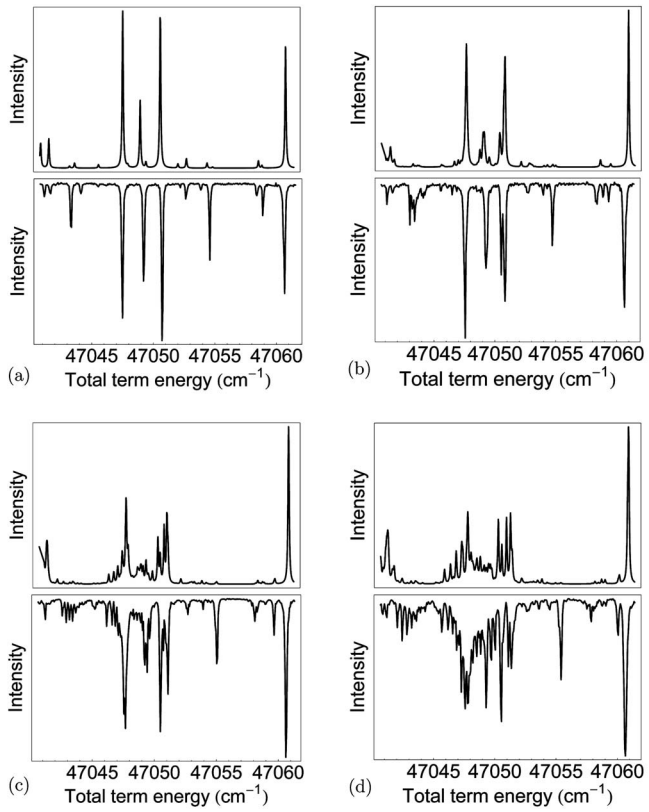

FIG. 6. Calculated (upper traces) and experimentally observed (lower traces) Stark effect in the double resonance spectra of the Rydberg states of CaF in the vicinity of $n^*=13$. Spectra are accessed through the $N'=3$ level of the $F'\,^2\Sigma^+$ intermediate state (accessed through an R pump transition from the ground state) in the pp polarization arrangement. The electric fields are (a) 0 V/cm, (b) 60 V/cm, (c) 120 V/cm, and (d) 180 V/cm. For the discussion of occasional disagreements between the observed and calculated transition intensities see Sec. V B.

basis states present in the intermediate state. The assumption of simplified ℓ-characters in the intermediate state eliminates interferences among the transition amplitudes of the different bright ℓ components, thereby simplifying the intensity patterns in the calculated spectra. We have also assumed that the transition intensity comes exclusively from transition amplitudes in which ℓ changes by ± 1. This assumption is not strictly valid for large Δn^* transitions since for large Δn^* the ℓ-changing transition dipole moment decreases and can become comparable to the permanent dipole moment (see Fig. 2). In addition, hydrogenic transition dipole moments were used for both core-nonpenetrating and core-penetrating states. These assumptions result in poorer agreement with the calculated intensities for some of the N^+ clusters. For example, the feature at 47 054.59 cm^{-1} in Fig. 6(a) belongs to the cluster with the nominal value of $N^+=6$. The intermediate $N'=3$ state in this case contains no $N^{+'}=6$ character because that would require f character and we have assumed that f character is negligible in the intermediate state. This absence of $N^{+'}=6$ character in the intermediate state results in a weaker transition intensity for this particular feature in the calculated spectrum. Its nonzero intensity comes from small $N^+<6$ character of the ℓ-admixed states in the nominally $g(-4)$ Rydberg state.

As the electric field is switched on, new states start to appear in both the calculated and experimentally observed spectra. This appearance of new features in the spectrum is due to electric-field-induced intensity borrowing from states that have bright character at zero-field. Since the electric-field-induced interaction among two states depends on the matrix elements between them and on their energy separation, unless two states that belong to two different values of N^+ are accidentally near degenerate, the strongest electric-field-induced interactions will be among the states that belong to the same N^+ complex. These new features, admixed by the field, are evident in Fig. 6(b). As the electric field increases, the number of states admixed by the field increases rapidly. In addition to intensity borrowing, the electric field causes energy shifts. Eventually, the electric field becomes strong enough to significantly mix states belonging to different N^+-clusters, and the agreement with our model worsens compared to that at low field [see Fig. 6(d)].

It is evident from the agreement between the calculated and the experimentally observed spectra that modeling the Stark effect in Rydberg states of CaF using an effective Hamiltonian approach is capable of capturing the main features of the low electric field, low-N Stark effect in molecular Rydberg states. All of the states needed for the long-range description are clustered around integer values of n^*, requiring inclusion of only a small number of core-penetrating states in the model in order to account for the core-penetration effects. When the electric field is sufficiently weak and N is sufficiently small, one does not need to include interactions with the neighboring n^* states. For NO,[18] it was reported that there is a negligible difference between the capability of a MQDT model and a matrix diagonalization method (which is more familiar to spectroscopists) to describe the low-field molecular Stark effect. We report here that the same is sufficient for CaF, which, unlike NO, has a molecular ion with a large dipole moment. The main difference between the NO and CaF effective Hamiltonian models is that the penetrating effects in our effective Hamiltonian are included by *ad hoc* parameters determined by the fit. Although the presence of the permanent ion-core dipole moment requires minor changes in the Hamiltonian, the treatment of the Stark effect in Rydberg states by an effective Hamiltonian matrix diagonalization method is the same as in nondipolar molecules.

C. Assignments

The calculated spectra were used to check the already published assignments and to make new ones. In order to facilitate the assignment procedure, we prepare stacked spectra at several different values of the electric field. These stacked spectra are prepared by plotting one above another several total term energy spectra originating from successive N' intermediate levels. In Fig. 7 we plot stacked spectra recorded from $N'=0$, 1, 2, and 3 at 0 and 70 V/cm. Since the abscissa is the total term energy, if a particular state is accessed from different intermediate states, this state will appear at the same total term energy in spectra accessed from states with different value of the N' quantum number. In zero-field spectra, because of the parity alternation as

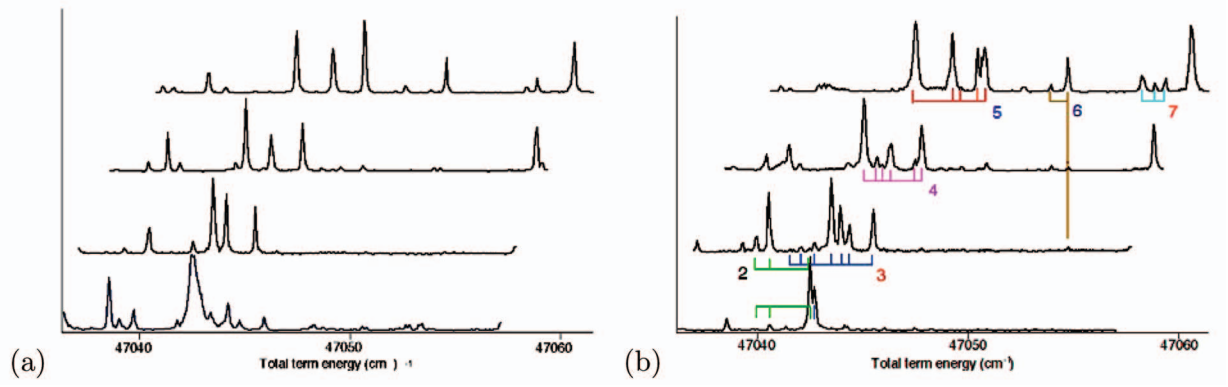

FIG. 7. Stacked double resonance spectra at (a) 0 V/cm and (b) 70 V/cm, recorded from $N'=0$, 1, 2, and 3 (bottom to top), in the *pp* polarization arrangement. Electric-field-induced mixing ($\Delta\ell=\pm1$, $\Delta N=0$, ±1, $\Delta N^+=0$) results in intensity borrowing and the appearance of new features in the spectrum. Transitions that terminate in different values of N^+ are color-coded according to the value of N^+, with the corresponding values of N^+ given in the same color on the plot.

$(-1)^{N^++\ell}$, the same state can only appear in two spectra recorded from intermediate state N' values differing by 2. However, since the electric field mixes states of opposite parity, in the presence of the electric field it becomes possible for the same Rydberg state to appear in spectra recorded from two consecutive values of N'. Interpretation of the spectrum recorded from $N'=0$ demands special attention. This spectrum is recorded using a $P(1)$ pump transition. The high density of spectral features in the P-branch of the $F'\,^2\Sigma^+\leftarrow X\,^2\Sigma^+$ transition usually does not permit using P-branches as pump transitions with this particular intermediate state, and only two assignments were made using the spectrum recorded from the $N'=0$ state. Both of these assignments have been confirmed in the analysis of the $R(0)$ spectrum recorded at 70 V/cm, where extra transitions induced by the Stark field appear in the spectrum.

When analyzing stacked spectra recorded in the presence of an electric field, we make the assumption that, in the absence of accidental degeneracies, N^+-intracluster mixing is stronger than $\Delta N^+=1$ intercluster mixing. This means that the first dark states to obtain intensity by electric-field-induced mixing will be the states of the same N^+ as the bright state. Since the transition intensity, when recorded from a particular N' level, varies from one value of final state N^+ to the next, and also varies within one N^+-cluster when accessed from a different N'-level [governed by the decomposition of the lower N' state in Hund's case (d) basis], there is going to be a particular value of N' most suitable for accessing each of the N^+ clusters (see Fig. 7). If there is an ambiguity whether a particular feature that appears in two spectra recorded from different values of N' is, in fact, the same state, the electric field tuning of both spectral features can be compared. Tables III–V contain the assignments of the $N\leqslant4$ and low-ℓ_R levels for f, g, and h states, made either by the Stark effect, polarization spectroscopy, or previously available.[6] For Stark-based assignments, the value of the zero-field energy is obtained by linear extrapolation of the energy to the zero-field value, unless the same state is accessible at zero field from a different value of N'.

TABLE III. Assignments of lowest-N, low-ℓ_R [denotes $\ell(\ell_R)$, where $\ell_R=N-N^+$ is the projection of ℓ on the ion-core rotational axis], f-states (cm^{-1}).

N	$f(-3)$	$f(-2)$	$f(-1)$
0	47 045.53		
1	47 047.77	47 044.15	47 042.51
2	47 050.71	47 046.27	47 043.52
3	47 054.20	47 049.20	47 045.07
4	47 058.49	47 052.96	47 047.50

D. Polarization dependence

Because of their rotational structure and strong ℓ-mixing, even in the absence of the external electric field, zero-field molecular Rydberg spectra will display a polarization dependence of the transition intensities that is different from the atomic case.[7] Because of the polarization dependence of the bright state character, when the Rydberg state spectrum is recorded in the presence of the electric field, the Stark spectrum of each Rydberg state also displays dependence on the polarization arrangement. In the absence of the external electric field, linear polarization can be used to distinguish Q transitions from P and R transitions (at the lowest values of N it is possible to distinguish P from R, as well). For example, in an $\omega_1+\omega_2$ double resonance experiment, with the ω_1 transition being an R transition, the ω_2 P or R transition will have stronger intensity when the ω_1 and ω_2 photons have parallel polarization than if their relative polarizations are perpendicular. On the other hand, if the ω_1 transition is R and the ω_2 transition is Q, the Q transition intensity will be stronger when the relative polarizations of the ω_1 and ω_2 photons are perpendicular. Similarly, circular polar-

TABLE IV. Assignments of lowest-N, low-ℓ_R, g-states (cm^{-1}).

N	$g(-4)$	$g(-3)$	$g(-2)$	$g(-1)$	g(0)
0	47 047.50				
1	47 050.63		47 044.07		
2	47 054.59	47 049.20	47 045.58	47 041.94	47 040.50
3	47 059.18	47 053.86	47 048.64	47 044.12	47 041.36
4	47 064.34	47 058.58	47 052.63	47 047.38	47 043.31

TABLE V. Assignments of lowest-N, low-ℓ_R, h-states (cm^{-1}).

N	$h(-5)$	$h(-3)$	$h(-1)$
0	47 049.79		
1	47 053.99	47 045.89	
2	47 058.89		47 042.56
3			47 044.56
4			

ization can be used to distinguish all three types of transitions [see Fig. 2(b) in Ref. 3]. Again, if the ω_1 transition is R, the ω_2 R transition will have stronger intensity if ω_1 and ω_2 photons have the same helicity. If the ω_1 is an R transition, and ω_2 a P transition, the transition intensity of ω_2 will be stronger when ω_1 and ω_2 photons have the opposite helicity. The intensity of the ω_2 Q transition will not differ between RHCP and LHCP polarizations of the ω_2 photon in this case.

The relative polarizations of the ω_1 and ω_2 photons in a double resonance excitation scheme determine the transition intensity into the state with bright character. In each N^+ cluster, in the general case, there might be more than one value of N with bright state character. The relative transition intensities for the three possible bright basis states ($\Delta N=0, \pm 1$) will be polarization dependent. In the presence of the electric field, the three transition amplitudes ($\Delta N=0, \pm 1$) will interfere, and the overall appearance of the Stark spectrum will be polarization dependent. The strength of the coupling caused by the Stark effect is much more strongly dependent on the energy separation among the interacting states than on small differences in the polarization dependence of the coupling matrix elements. However, in the two excitation steps, the difference between the energies of the three possible excitation pathways (driving P, Q, and R transitions) is small relative to the frequencies of the three possible transitions. Therefore, the effect of the polarization on the transition intensities, for a particular choice of ΔN, is stronger in the two excitation steps than in the Stark mixing step.

As the electric field is increased, N-mixing increases rapidly, and one would expect that the polarization dependence associated with a particular value of ΔN will be lost when the bright character of the three possible bright paths ($N-N'=0, \pm 1$) is uniformly distributed among the highly N-mixed states within one N^+ cluster. In Fig. 8 we show a part of a double resonance Stark spectrum around the integer value of $n^*=13$, recorded at 250 V/cm with $R(0)$ pump transition. The two spectra differ in the polarization arrangement (RHCP-RHCP-vertical versus RHCP-LHCP-vertical polarization arrangement). It is evident that, in this case, even though N is strongly mixed at 250 V/cm, the bright $f(-3)$ $N=0$ state is sufficiently distant from the other states of the $N^+=3$ cluster so that the polarization dependence associated with a P-type transition into the bright $N=0$ state is not completely lost in the region of the spectrum around 47 045.5 cm^{-1}. The region of the spectrum in which the intensity is enhanced in the RHCP-LHCP-vertical polarization arrangement is predominantly due to the $N'-1$ bright character (for the zero-field spectrum of this region, see the lowest trace in Fig. 4).

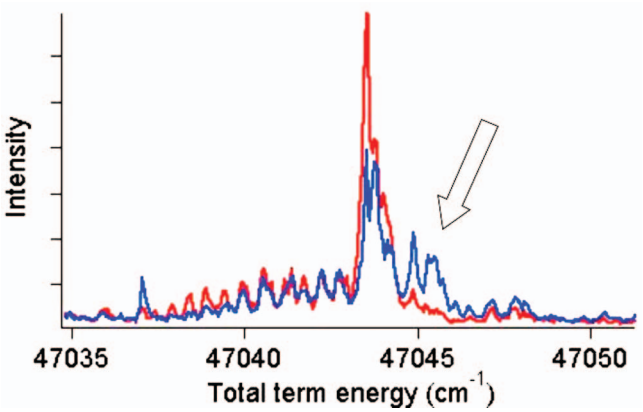

FIG. 8. Double resonance spectrum of CaF at 250 V/cm in the vicinity of $n^*=13$, recorded from $N'=1$ in RHCP-RHCP-vertical (red) and RHCP-LHCP-vertical (blue) arrangements. The arrow identifies the region in the spectrum where the N-mixing within a particular N^+ cluster due to the external electric field is incomplete, but polarization dependence associated with a p-type transition into the bright state is still preserved.

Thus the polarization dependence of the transition intensity provides insight into the mixing pathways within an N^+ cluster, but it is also possible to use the polarization dependence to observe examples of inter-N^+ cluster coupling. Figure 9 displays the same region of the spectrum as Fig. 8, but this time recorded using linear polarization. The red trace was recorded with the pp polarization arrangement and the blue trace with the ps polarization arrangement. Both spectra were recorded with the $R(0)$ pump transition and $E_{\text{Stark}}=250$ V/cm. The polarization arrangements employed in this experiment are capable of distinguishing Q transitions from P and R transitions. Since most of the bright Q transition character comes from the $f(-2)$ $N=1$ state at 47 044.15 cm^{-1}, which is near degenerate with many of the states that belong to the $N^+=3$ cluster, it is expected that the $f(-2)$ $N=1$ bright state character will be rapidly and uniformly distributed among the states in this $N^+=3$ cluster.

However, it is evident that only one feature in the spec-

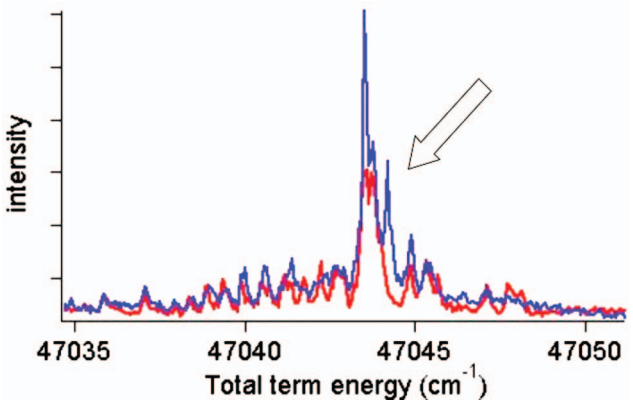

FIG. 9. Double resonance spectrum of CaF at 250 V/cm in the vicinity of $n^*=13$, recorded from $N'=1$ in pp (red) and ps (blue) arrangements. The arrow identifies a feature that exhibits a distinct Q-like polarization dependence at 250 V/cm, even though the surrounding features have lost the polarization dependence characteristic of a each ΔN value due to N-mixing induced by the field. This polarization behavior, different from other features in the $N^+=3$ cluster at the same electric field amplitude, is explained by an accidental degeneracy between two states that have different values of N^+.

trum in Fig. 9, at 47 044.21 cm^{-1}, displays a strong polarization dependence even at 250 V/cm and behaves like an almost pure Q transition. This state appears to be mixed with only one state in the $N^+=3$ cluster but not mixed with any other states in that N^+-cluster. It is conceivable that this is a result of an accidental degeneracy between two states belonging to different N^+ clusters. In fact, the $g(-1)$ $N=3$ state at 47 044.12 cm^{-1} that belongs to $N^+=4$ is almost degenerate with the bright-character bearing $f(-2)$ $N=1$ state at 47 044.15 cm^{-1}. The two states, although almost degenerate, cannot interact directly with each other in the presence of the external electric field, but this field can cause them to interact indirectly by coupling each of them to close-lying intermediaries. In cases like this it is difficult to make an unambiguous assignment because of interferences among the different $\Delta N=0, \pm 1$ transition amplitudes. Overall, the polarization dependence of the transition intensity distribution in a Stark spectrum of Rydberg states is useful for making assessments of both N^+ intra- and intercluster mixing pathways.

VI. SUMMARY

The ion-core N^+ rotational structure causes the molecular Rydberg electron to decouple from the ion core due to an external electric field in several stages. The separation of the stages of the decoupling depends on the molecular parameters, the strength of the electric field, and the n^* value at which the observation is made. We present here an analysis of the Stark effect in CaF in $n^*=13$. In this example it is possible to observe the first stage, in which both ℓ and N become mixed by the electric field before the N^+-mixing begins in the next stage. As N^+-mixing accompanies rotation-electronic interaction and ℓ-mixing by the ion-core multipole moments (especially severe in CaF, compared to H_2 and NO), the indirect interaction between the states of different values of N^+ as the external field increases, is enabled even before the field is gets strong enough to cause the direct N^+-mixing, through the interaction with the permanent dipole moment of the ion core.

We used the Stark effect at low electric field (<100 V/cm), under conditions where N^+ is conserved, to access the lowest rotational levels of f, g, and h states and to assign the actual or nominal value of their N^+ quantum numbers. The assignments rely on the large difference in size between the same-n^* transition dipole moment and the ion-core permanent dipole moment. In order to identify possible accidental degeneracies among the states that belong to different N^+-clusters, we used the dependence of the transition intensities on the relative polarizations of ω_1 and ω_2 linearly polarized photons in a double resonance experiment. Spectral features that exhibited polarization dependence distinct from expectations for a particular N^+-cluster were shown to belong to a different value of the N^+ quantum number. In the example where circularly polarized light was used, the polarization dependence of the transition intensities provided information about the N-mixing within a particular N^+-cluster.

An effective Hamiltonian was used to model the experimentally observed Stark effect. If the spectral window of interest is confined to the region of energy around an integer value of n^*, interactions with states from the neighboring n^* can be neglected. When this is the case, both effective Hamiltonian matrix diagonalization methods and MQDT perform equally well in describing the Stark effect in Rydberg states. The ℓ-decomposition obtained from the fit in this effective Hamiltonian demonstrates the importance of mixing of the core-nonpenetrating $g(-4)$ state with both an $f(-3)$ state and a core-penetrating $d\,^2\Sigma^+$ state. It is evident from Fig. 5 that this interaction is only discernible for lower-N rotational levels but could easily be missed when only $N>4$ levels are assigned.

In addition to describing the differences between the Stark effect in atomic and molecular Rydberg states, we applied the Stark effect to gain information about the extent of core penetration of some of the nominally core-nonpenetrating states. The analysis method for the low-field Stark effect on molecular Rydberg states presented here is limited by the 3 GHz experimental resolution in our optical-optical double resonance experiment. An optical-optical-microwave experimental scheme, which would provide resolution of several hundreds of kHz, would overcome the resolution limitations, and the analysis of the low-field Stark effect in such an experiment would provide information about values of the quantum number ℓ considerably higher than those presented here.

The analysis of the stages of the decoupling of the Rydberg electron from the body frame by the external electric field in molecular Rydberg states yields information about the gradual destruction of the barriers between different regions of state space. Knowledge on how the structure of the state space depends on the external electric field will be useful for rational design of experimental schemes that seek to control the population flow in state space. For example, since at low electric field all states belonging to a particular N^+-cluster are weakly coupled to states outside this cluster, it is possible, using a weak pulsed microwave field, to create a wavepacket composed of states with different values of ℓ, but having the same value of the N^+ quantum number. If a series of shaped low-amplitude microwave photons is applied, and the delay between them controlled, it would be possible to channel population into a particular ℓ, while keeping N^+ constant, in a similar manner to the one proposed for alkali-metal atoms.[37] Since the autoionization lifetimes are ℓ-dependent, such a scheme could exert or exploit control over lifetimes as well. Alternatively, instead of controlling the delay among the excitation pulses, varying the amplitude of the external field would permit an adiabatic change in state upon transit through an avoided crossing. Knowing the locations of avoided crossings among the states associated with different N^+-clusters, it is possible, by applying a somewhat stronger Stark field than in the first example, to adiabatically drive a $\Delta N^+=1$ process. In such a case, energy is transfered between the Rydberg electron and the ion core in two steps since ℓ gets destroyed before the strength of the field sufficient for causing the ΔN^+ is reached. In both cases, polarization can be used to suppress or enhance particular ΔN transitions. In both of these two examples, weak-field control schemes rely on knowledge on the state space struc-

ture and locations of resonances among the different types of motion and the propensity rules that govern the strength of interactions.

ACKNOWLEDGMENTS

This work has been supported by the National Science Foundation under Grant Nos. CHE-0450876 and CHE-0749821.

[1] C. M. Gittins, N. A. Harris, M. Hui, and R. W. Field, Can. J. Phys. **79**, 247 (2001).
[2] H. Lefebvre-Brion and R. W. Field, *The Spectra and Dynamics of Diatomic Molecules* (Elsevier Academic, San Diego, CA, 2004).
[3] V. S. Petrović and R. W. Field, J. Chem. Phys. **128**, 014301 (2007).
[4] S. N. Altunata, S. L. Coy, and R. W. Field, J. Chem. Phys. **123**, 084318 (2005).
[5] R. W. Field, C. M. Gittins, N. A. Harris, and C. Jungen, J. Chem. Phys. **122**, 184314 (2005).
[6] J. J. Kay, S. L. Coy, V. S. Petrović, B. M. Wong, and R. W. Field, J. Chem. Phys. **128**, 194301 (2008).
[7] T. F. Gallagher, *Rydberg Atoms* (Cambridge University Press, Cambridge, 1994).
[8] E. Luc-Koenig and A. Bachelier, J. Phys. B **13**, 1743 (1980).
[9] M. L. Zimmerman, M. G. Littman, M. M. Kash, and D. Kleppner, Phys. Rev. A **20**, 2251 (1979).
[10] K. Qin, M. Bistransin, and W. L. Glab, Phys. Rev. A **47**, 4154 (1993).
[11] G. R. Lloyd, S. R. Procter, E. A. McCormack, and T. P. Softley, J. Chem. Phys. **126**, 184702 (2007).
[12] H. H. Fielding and T. P. Softley, Phys. Rev. A **49**, 969 (1994).
[13] J. W. Cooper, E. B. Saloman, B. E. Cole, and Shardanand, Phys. Rev. A **28**, 1832 (1983).
[14] S. T. Pratt, E. F. McCormack, J. L. Dehmer, and P. M. Dehmer, Phys. Rev. Lett. **68**, 584 (1992).
[15] Y. Yamakita, S. R. Procter, A. L. Goodgame, T. P. Softley, and F. Merkt, J. Chem. Phys. **121**, 1419 (2004).
[16] W. L. Glab and J. P. Hessler, Phys. Rev. A **42**, 5486 (1990).
[17] E. Y. Xu, H. Helm, and R. Kachru, Phys. Rev. A **38**, 1666 (1988).
[18] A. L. Goodgame, H. Dickinson, S. R. Mackenzie, and T. P. Softley, J. Chem. Phys. **116**, 4922 (2002).
[19] J. B. M. Warntjes, F. Robicheaux, J. M. Bakker, and L. D. Noordam, J. Chem. Phys. **111**, 2556 (1999).
[20] T. Kobayashi, J. Geng, and M. Takami, Chem. Phys. Lett. **284**, 195 (1998).
[21] N. Nussenzweig and E. E. Eyler, J. Chem. Phys. **101**, 4617 (1994).
[22] N. J. A. Jones, R. S. Minns, R. Patel, and H. H. Fielding, J. Phys. B **41**, 185102 (2008).
[23] B. B. Clarson, S. R. Procter, A. L. Goodgame, and T. Softley, Mol. Phys. **106**, 1317 (2008).
[24] M. B. J. Chevaleyre, C. Bordas, and P. Labastie, Phys. Rev. Lett. **57**, 3027 (1986).
[25] P. F. Brevet, C. Bordas, M. Broyer, G. Jalbert, and P. Labastie, J. Phys. II **1**, 875 (1991).
[26] C. Bordas, P. F. Brevet, M. Broyer, J. Chevaleyre, P. Labastie, and J. P. Perrot, Phys. Rev. Lett. **60**, 917 (1988).
[27] G. Jalbert, P. Labastie, P. F. Brevet, C. Bordas, and M. Broyer, Phys. Rev. A **40**, 784 (1989).
[28] C. Bordas and H. Helm, Phys. Rev. A **45**, 387 (1992).
[29] J. M. Menédez, I. Martín, and A. M. Velasco, Phys. Rev. A **74**, 043413 (2006).
[30] G. R. Janik, O. C. Mullins, C. R. Mahon, and T. F. Gallagher, Phys. Rev. A **35**, 2345 (1987).
[31] C. R. Mahon, G. R. Janik, and T. F. Gallagher, Phys. Rev. A **41**, 3746 (1990).
[32] A. Osterwalder, R. Seiler, and F. Merkt, J. Chem. Phys. **113**, 7939 (2000).
[33] J. K. G. Watson, Mol. Phys. **81**, 277 (1994).
[34] C. Jungen and A. I. Roche, Can. J. Phys. **79**, 287 (2001).
[35] R. de L. Kronig, *Band Spectra and Molecular Structure* (Cambridge University Press, Cambridge, 1930).
[36] S. N. Altunata, S. L. Coy, and R. W. Field, J. Chem. Phys. **123**, 084319 (2005).
[37] H. Wen, C. Rangan, and P. H. Bucksbaum, Phys. Rev. A **68**, 053405 (2003).
[38] A. R. Edmonds, J. Picart, N. T. Minh, and R. Pullen, J. Phys. B **12**, 2781 (1979).